International Journal of Computational and Experimental Science and ENgineering (IJCESEN)

Vol. 11-No.4 (2025) pp. 9024-9034
http://www.ijcesen.com

Research Article

ISSN:2149-9144

Copyright © IJCESEN

Assessing the Effect of Blood Perfusion on Prostate Cancer Hyperthermia Using a Bioheat Simulation Approach

Soraya Bachaoui[1]*, Radja Khatir[2], Mohamed Issam Ziane[3], Abdelkader Belaidi[4]

[1]Medical Institute of Oran, University of Oran, Algeria.
* **Corresponding Author Email:** bachaoui.soraya@univ-oran1.dz - **ORCID:** 0009-0003-9602-1083

[2]Laboratory of Electrical Engineering and Materials (LGEM), 31000 Oran, Algeria
Email: khatir_radjaa@esgee-oran.dz - **ORCID:** 0009-0005-3819-6998

[3]Laboratory of Electrical Engineering and Materials (LGEM), 31000 Oran, Algeria
Email: ziane_issam@esgee-oran.dz - **ORCID:** 0000-0002-7048-7067

[4]National Polytechnic School of Oran ENPO Maurice Audin Algeria
Email: belaidiaek@gmail.com - **ORCID:** 0000-0002-5247-6650

Article Info:

DOI:10.22399/ijcesen.4352
Received: 05 July 2025
Revised: 20 November 2025
Accepted: 24 November 2025

Keywords

Hyperthermia,
Prostate cancer,
Blood perfusion,
Temperature Distribution,
Thermal damage.

Abstract:

The development of hyperthermia-based therapy for prostate cancer requires precise modeling of the thermal behavior of biological tissues. In order to simulate healthy tissue, this study creates a computational model of a prostate tumor that is shaped like a spherical area encircled by another concentric sphere. The investigation focuses on the effects of blood perfusion rate fluctuations on the temperature distribution and subsequent thermal damage in the surrounding tissue and tumor. The heating source is modeled as a collection of electric dipoles at the center of the tumor that are subjected to a microwave (2.45 GHz) alternating electromagnetic field. The temporal evolution of temperature and tissue necros is under varying perfusion rates is described using the Arrhenius damage model and the Pennes bioheat transfer equation. The findings contribute to the development of safer and more effective hyperthermia-based treatments for prostate cancer by offering a quantitative understanding of the effects of blood flow on heat diffusion and necrotic percentage

1.Introduction

Because of their biological complexity and inconsistent responsiveness to treatment approaches, the majority of human cancers are still incurable after decades of research and multiple clinical trials [1-5]. One of the most prevalent cancers in males, prostate cancer is being treated with a variety of methods, including chemotherapy, external radiation therapy, and radical prostatectomy. Nevertheless, these traditional treatments frequently have poor results and cause serious harm to nearby healthy organs [6–9]. Accurately treating the tumor–tissue contact is crucial for effective tumor control because failing to do somay cause local recurrence [10,11].

By raising radiosensitivity and enhancing the overall therapeutic result, hyperthermia which involves heating tumor tissue to temperatures between 41 and 46 degrees Celsius is known to improve the effectiveness of radiation therapy [12–16]. For the treatment of locally advanced or recurring prostate cancer, combined thermoradiotherapy has sodrawn a lot of interest. The synergistic advantages of combining ionizing radiation and regulated heating have been validated by both clinical and experimental studies [17]. However, due to the prostate's intricate shape and high blood perfusion rate, perfect heat regulation in this organ is still difficult to achieve [18]. As a heatsink, excessive blood flow lowers

local temperatures and lessens the therapeutic impact.

Two promising methods for producing localized warmth in deep-seated tumors are magnetic and microwave hyperthermia. First described by Gilchrist et al. (1957) and then refined by Gordon et al. (1970s), magnetic hyperthermia is based on magnetic nanoparticles that, when exposed to an alternating magnetic field, transform electromagnetic energy into heat [19–21].

By raising the tumor temperature to lethal levels (over 43 °C), this targeted heating can harm cancer cells while protecting healthy tissues [22–24]. Such targeted thermal augmentation enables lower radiation doses and less collateral damage to vital organs like the bladder or spinal cord when paired with chemotherapy or radiotherapy. The quantity of heat deposited into the tumor and the physiological processes that disperse this heat, including blood circulation, are key factors in the success of hyperthermia [25]. As a natural cooling process, blood circulation removes heat from the treated area and has a big impact on temperature consistency. As part of the body's thermoregulatory response, the perfusion rate rises with temperature, preventing heat from spreading into healthy tissue [26–28]. Therefore, in order to effectively forecast temperature and damage, spatially variable blood perfusion must be incorporated into any meaningful computer model for hyperthermia [29,30].In this regard, numerical simulations are crucial instruments for developing, refining, and evaluating hyperthermia therapy plans prior to their practical application. They make it possible to precisely assess how heat moves through tumors and healthy tissue, as well as how varying perfusion rates affect the effectiveness of treatment.In order to clarify the connections between variations in blood perfusion rate, heat source distribution, heat generation, and temperature change within a model tumor, this work uses three-dimensional computer models. The goal of the study is to improve our knowledge of temperature distributions, which are difficult to measure experimentally.This paper suggests incorporating a variable blood perfusion rate, a quantity that directly affects the computation of temperature distribution in biological tissues, into the Pennesbioheate equation.An array of heated electrical dipoles placed in the middle of a prostate cancer tumor produces local hyperthermia, which is the subject of the paper's phenomenological investigation. The fundamental idea behind this medical procedure is to maintain a steady temperature in the targeted tumor tissue between 42°C and 50°C [31, 32, 33] for a long enough period of time to kill the tumor mass while preserving the nearby healthy tissues and organs [34]. The thermal diffusion of heat produced by the sources within the impacted area causes the cellular temperature to rise. A number of physical factors that can affect the thermal effect during treatment control this thermal diffusion.

The first section examines how the temperature of these electric dipoles inside the tumor changes in response to different blood perfusion rates. Within the microwave range, 2.45×10^9 Hz is the applied frequency.

The best maximum temperature is examined in the second section utilizing two different array designs (2x2x2) and (3x3x3), all while keeping the spacing between the individual electrical dipoles constant.

2. Methodology

2.1The physical model

Two concentric spheres were used to idealize the prostate geometry: the outer sphere (radius r_2=40 mm) represented the surrounding healthy tissue and the inner sphere (radius r_1=25 mm) represented the tumor.

As a result, the outer layer is consistently 15 mm thick. Throughout the simulation, the thermophysical characteristics of the blood and tissues were taken to be constant, and both media were regarded as homogeneous and isotropic (Tables 1-2).

Electric dipoles at the tumor center are used as the model for the heating sources. The regular arrays of 2x2x2 and 3x3x3 dipoles are spaced 0.25 mm apart in all three spatial directions (x, y, and z). When exposed to a microwave-frequency alternating magnetic field at $f = 2{,}45\,.\,10^9$ Hz, each dipole transforms electromagnetic energy into thermal energy.

Table 1. *Thermophysical properties of Healthy Tissue (Prostate) and Tumor [35,36,37]*

Materials	**Properties**			
	Thermal conductivity (W/m.K)	Density (Kg/m^3)	Constant pressure heat capacities [J/(kg.k)]	Electrical conductivity σ(S/m)
Healthy Tissue (Prostate)	0.51	1045	3760	3
Tumour	0.51	1045	3779	3

Table 2. *Thermophysical Properties of Blood [36, 38, 39]*

Name	**Expression**	**Value**	**Description**

Rho-blood	1000	1000 [kg/m^3]	Blood Density
Cp-blood	3639[J /kg.k]	3639 [J/kg.k]	Specific heat of the Blood
Omega-blood	Variant [l/s]	Variant [l/s]	Blood perfusion rate
T-blood	37 [deg C]	310.2 [K]	Blood Temperature

2.2 The governing equations

The Pennes bioheat transfer equation [40,41] describes the temperature evolution inside the tumor and surrounding tissue:

In the tumor $0 \leq r < r_1$

$$\rho_1 c_1 \frac{\partial T_1}{\partial t} + \nabla(-k_1 \nabla T_1) = \rho_b c_b w_b (T_b - T_1) + Q_m + Q_{ext} \quad (1)$$

in healthy tissue $r_1 \leq r < r_2$

$$\rho_2 c_2 \frac{\partial T_2}{\partial t} + \nabla(-k_2 \nabla T_2) = \rho_b c_b w_b (T_b - T_2) + Q_m \quad (2)$$

where tissue density [kg/m3] is represented by ρ. c-specific heat [J/kg.K], k-thermal conductivity [W/m.K], T-local temperature [°C], Q_m-metabolic heat generation (not included here), Q_{ext}-volumetric heat source from the electromagnetic field [W/m^3], w_b-blood perfusion rate (s^{-1}),ρ_b, c_b, T_b-density, specific heat, and blood temperature, respectively. The term $c_b w_b (T_b - T)$ accounts for the removal of heat within the tissue due to the blood perfusion.

The formula for the external heat generation term is:

$$Q_{ext} = \sigma |E|^2 \quad (3)$$

where E is the local electric field intensity and σ is the tissue's electrical conductivity (S/m).The metabolic term $Q_{met}$was left out of the computations since it is orders of magnitude smaller than the external heat source.

2.3 Initial conditions and boundaries

The following presumptions and restrictions were accepted:

• Initial temperature: all tissues are at body temperature prior to heating.

$$T(r, t = 0) = 37℃$$

• Symmetry condition: the tumor center's temperature stays fixed.

$$\left.\frac{\partial T}{\partial r}\right|_{r=0} = 0$$

• Interface continuity: At the tumor-tissue boundary, the temperature and heat flow are constant.

$$T_t = T_h, \quad k_t \frac{\partial T_t}{\partial r} = k_h \frac{\partial T_h}{\partial r}$$

• Outer boundary: natural convection causes heat loss.

$$-k \left.\frac{\partial T}{\partial r}\right|_{r=r_2} = h(T - T_\infty)$$

with an ambient temperature T_∞ = 37 °C and a convection coefficient h = 10 W.m^{-2}. k^{-1}.

The electromagnetic field exposure time was set at t = 600 s (10 min).

2.4Model of blood perfusion and thermal damage

We looked at six blood perfusion rates:

$$w_b = \{48, 1.0x10^2, 1.8x10^2, 2.6x10^2, 3.6x10^2, 3.6x10^3\} s^{-1}$$

These values represent typical physiological and pathological ranges for prostate tissues [35-38].

The Arrhenius damage integral was used to quantify thermal injury [42,43]:

$$\Omega(t) = \int_0^t A \exp\left(-\frac{E_a}{RT(t)}\right) dt \quad (4)$$

Where A is the frequency factor (3,1 x 10^{98} s^{-1}), Ea is the activation energy for irreversible tissue denaturation (6.3 x 10^5 J/mol), and R = 8,314 J.mol^{-1}.k^{-1} is the universal gas constant.

The relationship between Ω and the necrotic fraction θ of the tissue is as follows:

$$\theta = 1 - e^{-\Omega}$$

Complete necrosis is indicated by θ =1

2.5 Use of numerical methods

The finite element method (FEM) was used to numerically solve the model equations.

With a minimum element size of 0.1 mm close to the tumor-tissue interface and 1 mm in the outer regions, a free tetrahedral mesh was employed.

A backward implicit differentiation method with a time step of 0.1 s was used to discretize time.

When the relative temperature error between iterations was less than 10^{-5}, convergence was reached.

Tables 1 and 2 provide a summary of the thermophysical parameters of the blood and tissues.

Only the perfusion rate was changed to isolate its impact on temperature and necrosis; all other simulations were run with the same material properties.

By contrasting the steady-state temperature profiles with previously released experimental and computational data [36, 44], the model was confirmed to have comparable maximum temperature values and consistent spatial distributions.

3. Results

After ten minutes of exposure for different blood perfusion rates, Figure 1 shows the three-dimensional temperature distribution in both tumor and healthy tissue. Different maximum and minimum temperature profiles that are highly dependent on the perfusion rate are shown in each simulation.

The lowest temperatures, which range from 37 °C to 40 °C, are noted at the outer edge of the healthy tissue. The surrounding healthy tissue heated above 40 °C for the two lowest perfusion rates (W_1 = 48 s^{-1} and W_2 = 1×10^2 s^{-1}) because there was not enough blood flow to dissipate the heat produced at the tumor center (Fig. 1a–b).

The heat removal becomes more efficient as the perfusion rate rises ($W_3 = 1.8\times10^2$ s^{-1}, $W_4 = 2.6\times10^2$ s^{-1}, $W_5 = 3.6\times10^2$ s^{-1}, and $W_6 = 3.6\times10^3$ s^{-1}), resulting in lower and more consistent temperatures in the healthy tissue that are near physiological levels (≈37 °C). As a result, increased perfusion rates considerably lessen tissue damage (Fig. 1c–f).

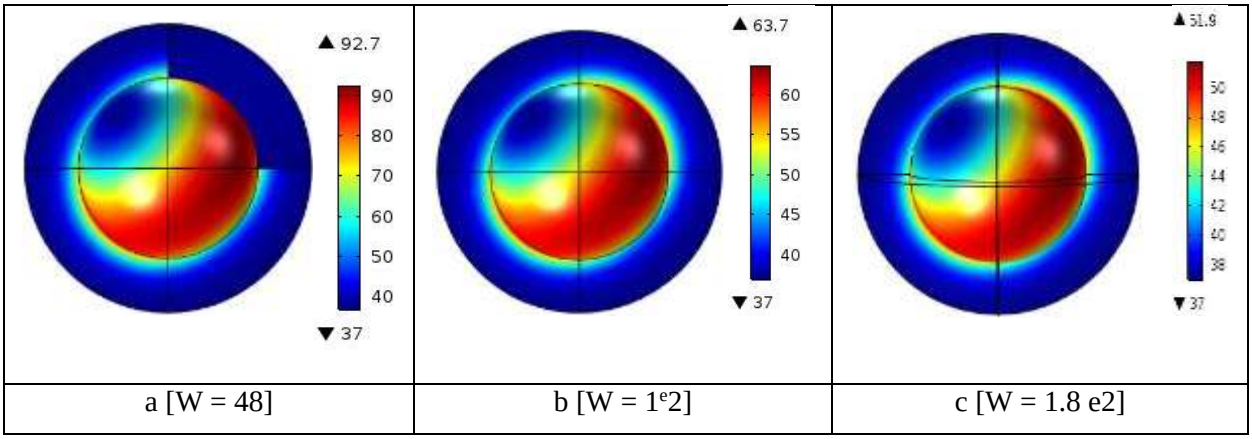

a [W = 48]	b [W = 1^{e}2]	c [W = 1.8 e2]

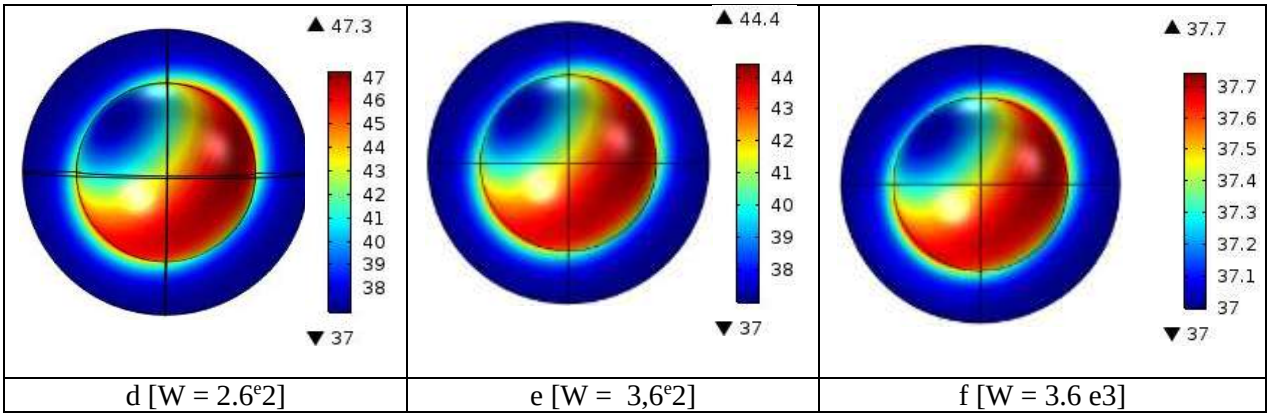

d [W = 2.6^{e}2]	e [W = 3,6^{e}2]	f [W = 3.6 e3]

Figure 1 *Representation of the surface temperature distribution on healthy tissue and Tumor as a function of blood perfusion rate [a(W_1 = 48 [1/s]), b (W_2 = 1e2 [1/s]), c (W_3=1.8e2 [1/s]), d (W_4 = 2.6e2 [1/s]), e (W_5= 3.6e2 [1/s]),f (W_6 = 3.6e3 [1/s])].*

Near the heat source region, the highest temperatures range from 90 °C (low perfusion) to 37.7 °C (high perfusion). While examples W_4–W_6 keep the tumor below the coagulation threshold because of excessive cooling by perfusion, cases W_1–W_3 are efficient in attaining total tumor ablation because tumor coagulation often demands temperatures above 50 °C [44]. The therapeutic temperature window is thus crucially controlled by the perfusion rate.

The radial temperature variation along particular lines that cross the tumor and healthy tissue is shown in Figures 2 and 3.

The temperature distribution inside the tumor is depicted in Figure 2 along the line that connects the sites $M_1(0, 25, 15)$ and $M_2(25, 0, 15)$, which are 15 mm above the tumor center. As the perfusion rate rises, the peak temperature in the center band gradually drops, demonstrating that improved blood flow reduces local overheating and speeds up cooling.

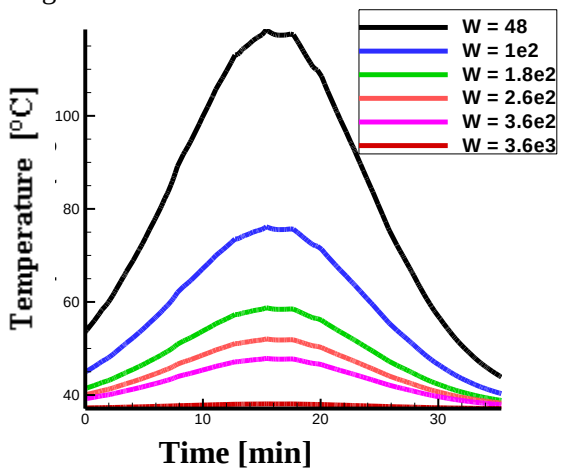

Figure 2 *the evolution of the radial temperature of the tumor cell according to the band Central and based on different values of the Infusion rate [W].*

The temperature gradient along the y-axis (z = 15 mm) through the healthy tissue is shown in Figure 3. The temperature at the tumor boundary rises over 40 °C for low perfusion levels ($W_1 = 48$ s^{-1} and $W_2 = 1\times10^2$ s^{-1}), and a significant amount of the healthy area is warmed. The tumor reaches about 51 °C with moderate perfusion ($W_3 = 1.8\times10^2$ s^{-1}), which is still enough for necrosis but still shows some heat diffusion into the surrounding tissue.

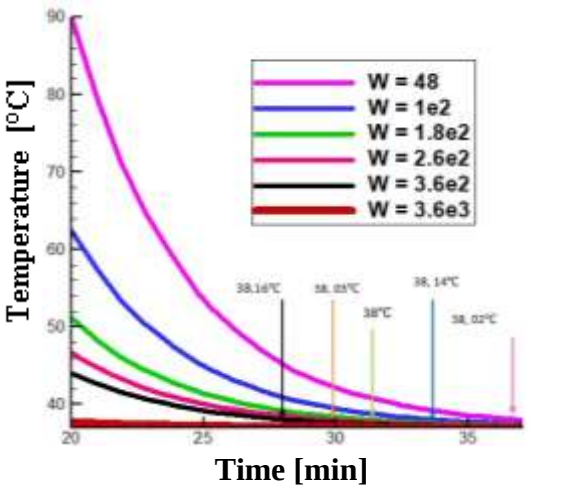

Figure 3 *The evolution of radial temperature on healthy tissue [next the y-axis between the two points (0,40,15) and (0,20,15)] and for different Infusion rate*

The heated zone narrows as perfusion rises ($W_4 = 2.6\times10^2$ s^{-1} and $W_5 = 3.6\times10^2$ s^{-1}), with tissue above y = 17–19 mm staying near 37 °C. Nearly the whole outer layer remains at physiological temperature at the maximum perfusion rate ($W_6 = 3.6\times10^3$ s^{-1}), demonstrating total protection of the healthy area from heat diffusion.

The temporal variation of temperature at various fixed sites within the tumor and healthy tissue is shown in Figure 4. The temperature close to the tumor surface is always higher than the surrounding areas for a given perfusion rate, and it progressively drops toward the outer boundary.

In low and moderate perfusion situations (W_1–W_5), the outside surface approaches 37 °C and reaches steady-state conditions during the first minute of exposure, whereas the interface temperature between the tumor and healthy tissue stays over 40 °C during the heating duration.The interface and peripheral temperatures, on the other hand, stay almost constant at body temperature for the maximum perfusion rate ($W_6 = 3.6\times10^3$ s^{-1}), demonstrating that high perfusion inhibits any appreciable thermal accumulation. These findings show how blood flow stabilizes temperature distribution and plays a critical role in determining the effective heating zone. The necrotic tissue fraction for each perfusion case was calculated using the Arrhenius model in order to measure the biological impact of heating. The geographical distribution of necrosis in a 2D slice (yoz-plane) of the tumor is displayed in Figure 5.The necrotic fraction achieves its greatest value ($\Omega \approx 1$) near the tumor core at low perfusion ($W_1 = 48$ s^{-1}), signifying total heat destruction. But a sizable amount of nearby healthy tissue is also impacted. The extent of necrosis diminishes with increasing perfusion: at $W_4 = 2.6\times10^2$ s^{-1} and $W_5 = 3.6\times10^2$ s^{-1}, the tumor necrosis becomes incomplete while the healthy region is mostly intact.At intermediate perfusion rates ($W_2 = 1\times10^2$ s^{-1} and $W_3 = 1.8\times10^2$ s^{-1}), the best compromise is found, where tumor elimination is almost complete and surrounding tissue damage is at its lowest. On the other hand, tumor damage is minimal at the maximum perfusion ($W_6 = 3.6\times10^3$ s^{-1}) because the strong cooling impact inhibits adequate heat accumulation.By displaying the time evolution of the necrotic fraction at multiple sites from the tumor boundary to the healthy tissue, Figure 6

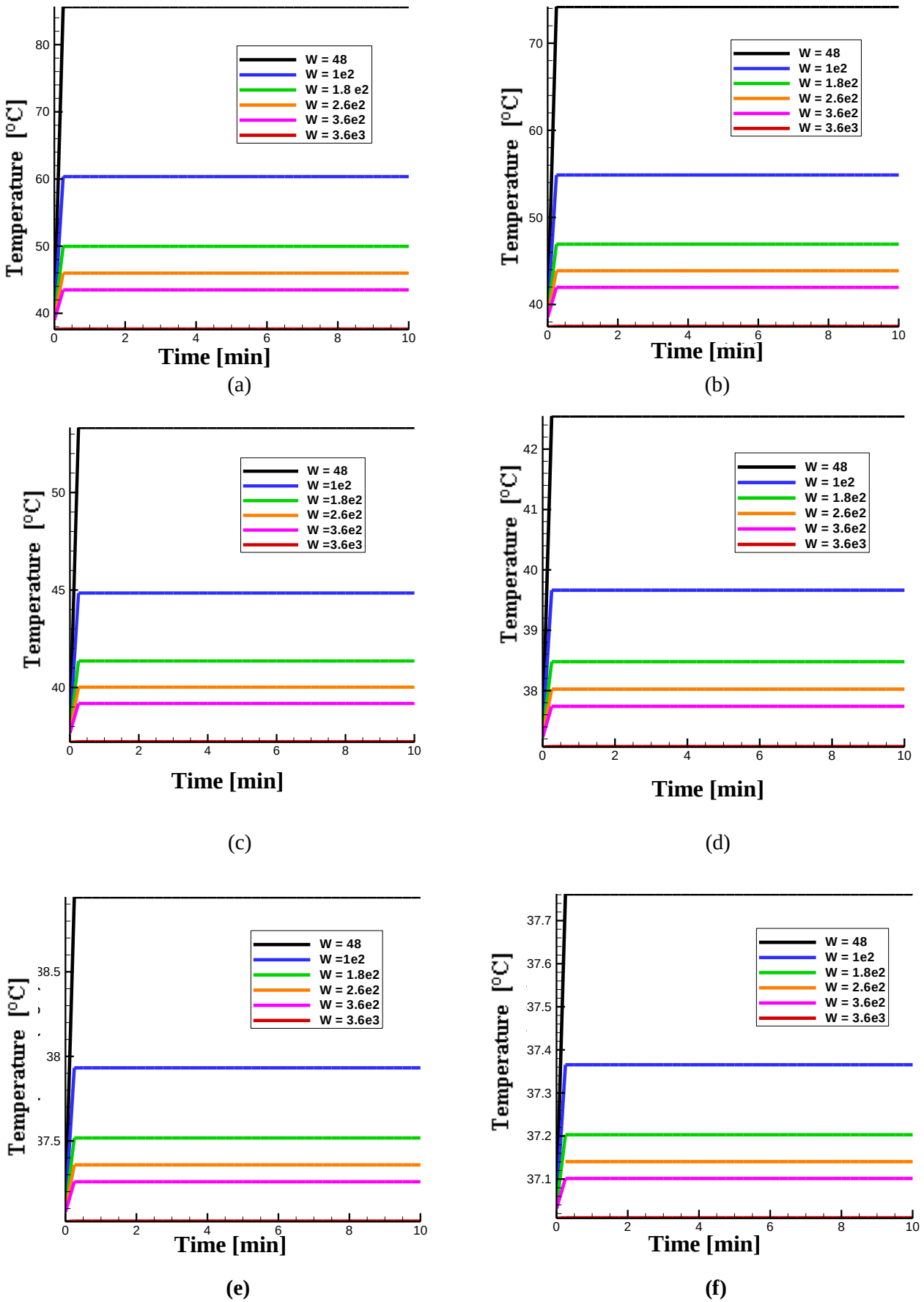

Figure 4 *Evolution of the temporal temperature at different fixed points [a (0,0,24), b (0,0,25), c(0,0,28), d(0,0,32), e(0,0,36), f(0,0,40)]*

validates these findings. Necrosis spreads broadly in both areas when perfusion rates are poor. The degree of thermal damage in healthy tissue gradually decreases as perfusion rises, eventually becoming insignificant. Necrosis is completely contained inside the tumor volume for $W \geq 2.6\times10^{2}$ s^{-1}, guaranteeing selective heating.The necrotic fraction achieves its greatest value ($\Omega \approx 1$) near the tumor core at low perfusion (W_1 = 48 s^{-1}), signifying total heat destruction. But a sizable amount of nearby healthy tissue is also impacted. The extent of necrosis diminishes with increasing perfusion: at $W_4 = 2.6\times10^{2}$ s^{-1} and $W_5 = 3.6\times10^{2}$ s^{-1}, the tumor necrosis becomes incomplete while the healthy region is mostly intact.

At intermediate perfusion rates ($W_2 = 1\times10^{2}$ s^{-1} and $W_3 = 1.8\times10^{2}$ s^{-1}), the best compromise is found, where tumor elimination is almost complete and surrounding tissue damage is at its lowest. On the other hand, tumor damage is minimal at the maximum perfusion ($W_6 = 3.6\times10^{3}$ s^{-1}) because the strong cooling impact inhibits adequate heat accumulation.

By displaying the time evolution of the necrotic fraction at multiple sites from the tumor boundary to the healthy tissue, Figure 6 validates these findings. Necrosis spreads broadly in both areas when perfusion rates are poor. The degree of thermal damage in healthy tissue gradually decreases as perfusion rises, eventually becoming insignificant. Necrosis is completely contained inside the tumor volume for $W \geq 2.6\times10^{2}$ s^{-1}, guaranteeing selective heating.

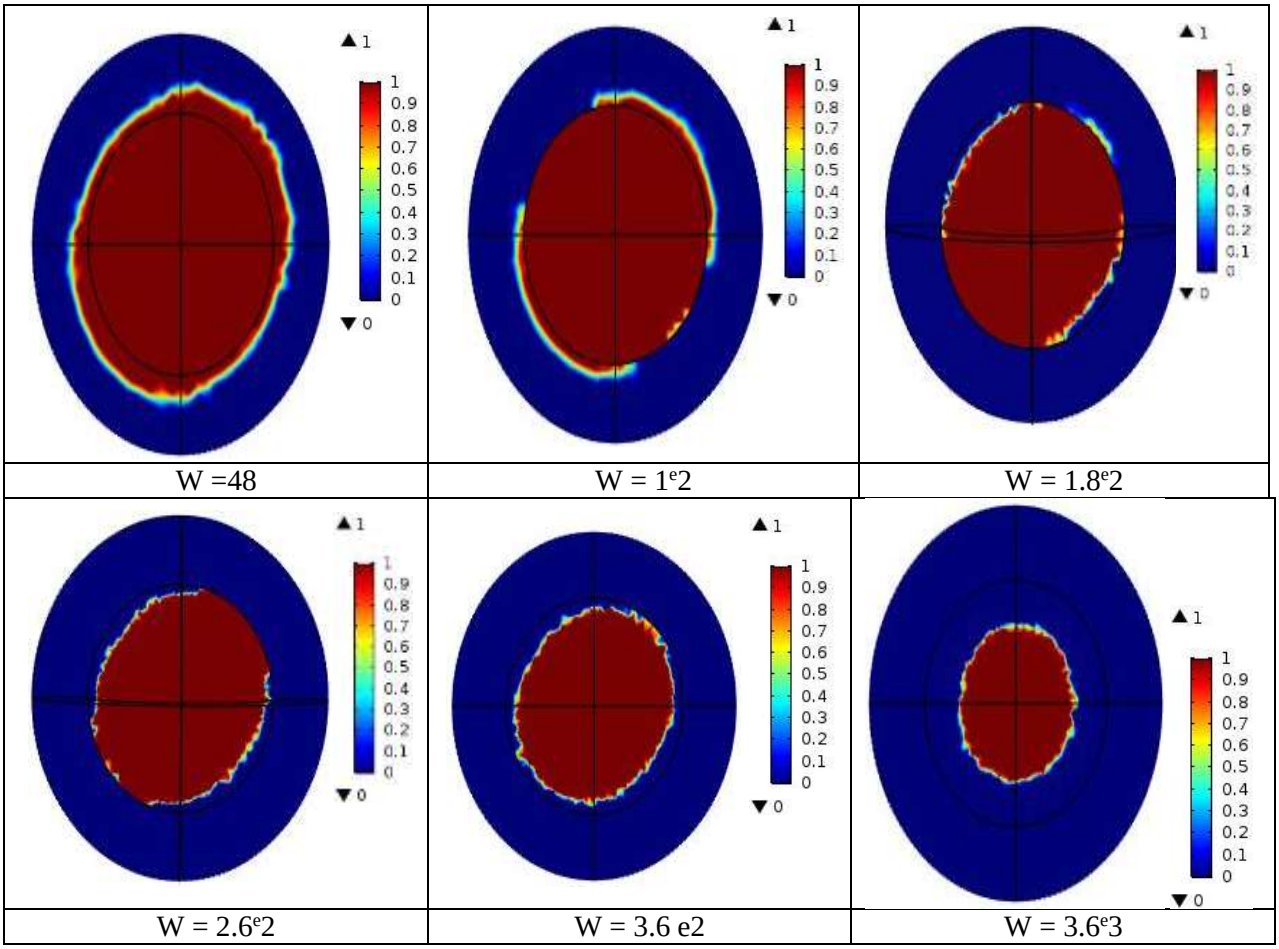

Figure 5 *Fraction of necrotic tissue on a slice cut according to the YOZ Plan as a function of different Infusion rate [a (W_1 = 48 [1/s]), b ($W_2 = 1^{e}2$ [1/s]), c (W_3=1.8^{e}2 [1/s]), d (W_4 = 2.6e2 [1/s]), e (W_5= 3.6e2 [1/s]), f ($W_6 = 3.6^{e}3$ [1/s])].*

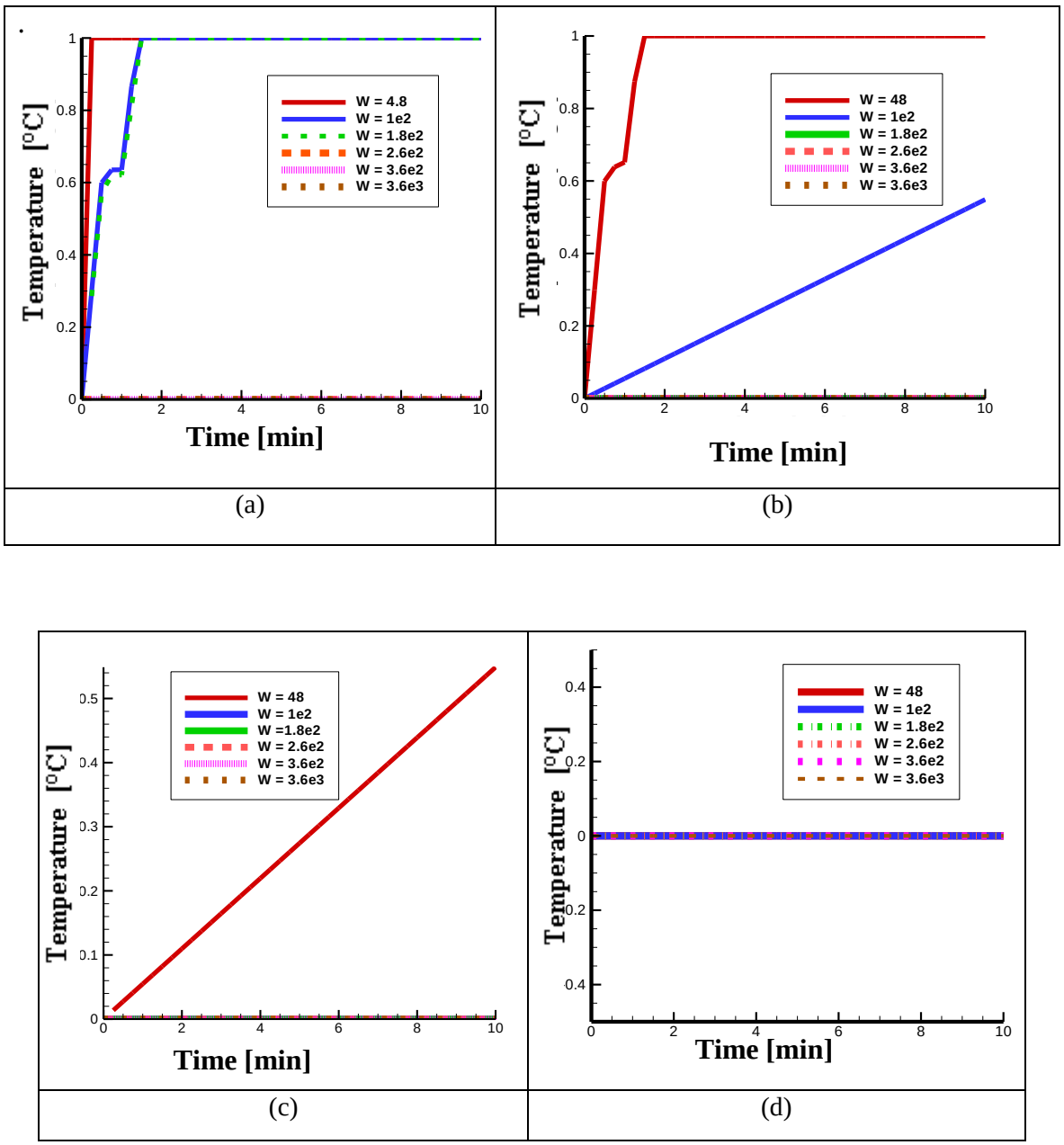

Figure 6 *Evolution of the necrotic fraction as a function of time in Healthy Tissue [a (0,0,24), b (0,0,27), c (0,0,30), d (0,0,40)].*

4. Discussion

The current work used a model of prostate tissue exposed to localized electromagnetic hyperthermia to examine the spatiotemporal progression of temperature and thermal damage. The findings show that blood perfusion rate is a key factor in regulating the temperature increase inside the tumor and the surrounding healthy tissue, as well as its spatial extent.

The produced heat is not effectively dispersed by blood flow at low perfusion rates (48–1.8×10² s^{-1}), which causes a noticeable rise in temperature both inside the tumor and in surrounding tissues. These situations result in a sharp increase in temperature to cytotoxic levels (>50 °C), which efficiently kill tumor cells but run the danger of scorching the peritumorous area. Although there is a significant chance of collateral harm, such circumstances are appropriate for total tumor ablation.

The constant intake of colder blood functions as a heat sink at greater perfusion rates (≥2.6×10² s^{-1}), greatly lowering the peak temperature and the radial temperature gradient. Because the temperature in healthy tissue stays near physiological levels (37–38 °C), the treatment is therefore safer. However, because of the substantial cooling impact, the temperature cannot exceed the coagulation threshold when perfusion is severe (3.6×10³ s^{-1}), which leads to incomplete tumor heating. These results are consistent with earlier research on the thermoregulatory behavior of

biological tissues [24,25,36].

Regardless of perfusion level, steady-state conditions are reached within the first minute of exposure, according to the temperature–time curves in Figure 5. This brief stabilization period demonstrates that rapid energy deposition in the target volume is facilitated by electromagnetic heating. To guarantee irreversible tissue damage, as indicated by the Arrhenius integral, therapeutic temperatures must be maintained for the recommended amount of time (10 minutes).

Figures 5–6, which analyze the necrotic proportion, provide additional evidence for these findings. According to the Arrhenius-based damage model, high perfusion limits necrosis to the tumor core, but poor perfusion causes widespread necrosis outside the tumor margin. Complete tumor ablation with no harm to healthy tissue is the best balanced result from the middle perfusion range (1.0×10^{2}–2.6×10^{2} s^{-1}). Realistic physiological parameters for prostate tissue are reflected in this ideal range [35–38].

Practically speaking, these findings emphasize how crucial it is to take patient-specific perfusion variability into consideration when designing a treatment plan. To obtain comparable therapeutic dosages, people with more vascularization might need to be exposed for longer periods of time or expend more energy. On the other hand, in order to prevent overheating, patients with limited perfusion could require less power.

Furthermore, comparing the two dipole networks (2×2×2 and 3×3×3) sheds light on how heat source dispersion affects.

While more dipoles improve thermal uniformity, they also raise the possibility of damaging healthy tissue in the event of inadequate perfusion (fig.7). Wider necrotic zones resulted from the simulations' increased temperatures at the tumor's periphery caused by the (3×3×3) shape (Fig.8, 9). Only when paired with high perfusion ($\geq2.6\times10^{3}$ s^{-1}) (Fig.10, which enhances convective heat loss to offset excessive heating, can this combination become beneficial.

Overall, the study demonstrates that the final temperature distribution and tissue response are determined by the interaction between blood circulation and electromagnetic energy deposition. For the purpose of creating customized hyperthermia procedures, the model thus offers a helpful forecasting tool. Clinicians can minimize side effects and maximize therapy success by modifying heat source geometry and perfusion-related parameters.

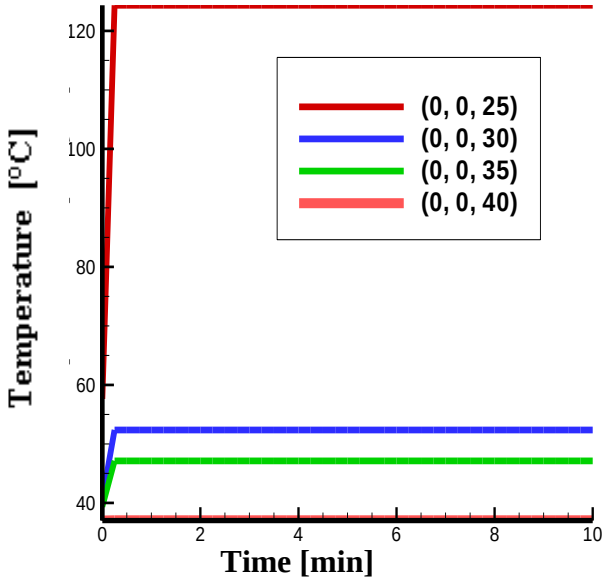

Figure 7 *The temporal evolution of the temperature at different points (Z direction). [(0,0,25), (0,0,30), (0,0,35), (0,0,40)] provided by a network of 3x3x3 sources of heating (electric dipoles) of distance d = 0.25 mm. (w =* $2.6e2\ [1/s]$)

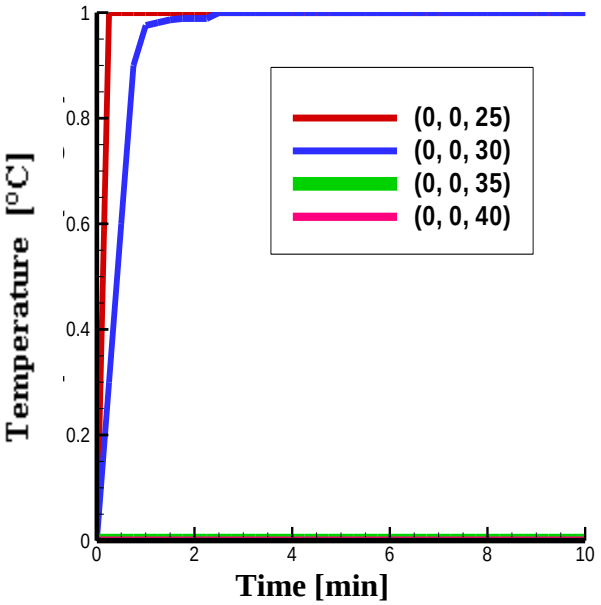

Figure 8 *Temporal evolution of the necrotic fraction at different points (Z direction). [(0,0,25), (0,0,30), (0,0,35), (0,0,40)] provided by a network of 3x3x3 sources of heating (electric dipoles) distance d = 0.25 mm (w =* $2.6e2\ [1/s]$)

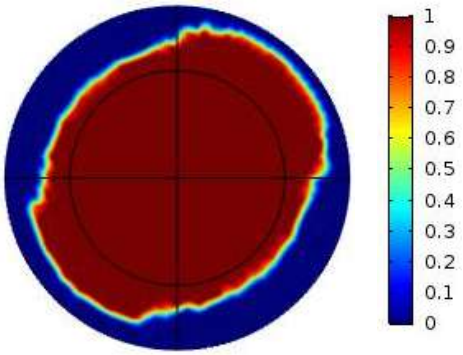

Figure 9 *Fraction of the necrotic tissue on a slice cut according to the YOZ Plane in the 3x3x3 network with a distance of d = 0.25 mm between the heat sources. . (*$w = 2.6e2\ [1/s]$*)*

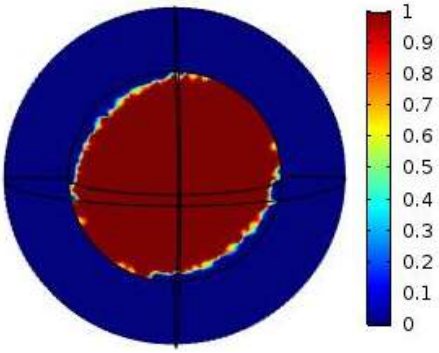

Figure 10 *Fraction of the necrotic tissue on a slice cut according to the YOZ Plane in the 3x3x3 network with a distance of d = 0.25 mm between the heat sources. . (*$w = 2.6e3\ [1/s]$*)*

5. Conclusions

The combined effects of blood perfusion and electromagnetic heating on temperature distribution and tissue necrosis were examined in this work using a computational model of prostate tumor hyperthermia. Two dipole configurations (2×2×2 and 3×3×3 arrays) were simulated using the Arrhenius damage model and the Pennes bioheat equation.

The findings support the notion that blood perfusion is a vital physiological factor that influences the safety and effectiveness of therapies for hyperthermia.

• Tumor necrosis is complete at low perfusion rates ($\leq 1.8\times10^2\ s^{-1}$), but there is also a noticeable warming of healthy tissue.

• Heat dissipation hinders adequate tumor heating at high perfusion rates ($\geq 3.6\times10^2\ s^{-1}$), resulting in partial ablation.

• The perfusion rate of $2.6\times10^2\ s^{-1}$ is the ideal treatment window, since it guarantees sufficient tumor destruction while keeping healthy tissue at body temperature.

The computational results show that selective heating of the tumor and preservation of surrounding tissue are made possible by a suitable balance between energy input and perfusion rate. A useful design and optimization tool for upcoming advancements in hyperthermia therapy for prostate cancer may be this predictive model.

Future research should concentrate on combining time-dependent and heterogeneous perfusion models, more accurately linking the thermal and electromagnetic fields, and confirming the predictions using clinical or experimental data.

Author Statements:

- **Ethical approval:** The conducted research is not related to either human or animal use.
- **Conflict of interest:** The authors declare that they have no known competing financial interests or personal relationships that could have appeared to influence the work reported in this paper
- **Acknowledgement:** The authors declare that they have nobody or no-company to acknowledge.
- **Author contributions:** The authors declare that they have equal right on this paper.
- **Funding information:** The authors declare that there is no funding to be acknowledged.
- **Data availability statement:** The data that support the findings of this study are available on request from the corresponding author. The data are not publicly available due to privacy or ethical restrictions.

References

[1] Glustini AJ, Petryk AA, Cassim SM, Tate JA, Baker I, Hoopes P J(2013) Magnetic Nanoparticle Hyperthermia In Cancer Treatment. Nano Life 2010. Author manuscript: available in PMC 10 decembre2013.

[2] Anupma M, Surita M, Sanjay M (2009) Microwave Interstitial Tumor Ablation: New modality for treatment of Liver Cancer. Except from the Proceedings of theComsol Conference 2009

Bangalore.
[3] Lu X Q, Burdette E C, Bornstein B A, Hansen J L, Svensson G K (2009) Design of an ultrasonic therapy system for breast cancer treatment. Int.J. Hyperthermia, 12(3): 375–99.
[4] Tsuda N, Kuroda K, Suzuki Y (1996) An inverse method to optimize heating conditions in RF-capacitive hyperthermia. IEEE Trans Biomed Eng, 43(10): 1029-1037.
[5] Chen Z P, Roemer R B, Cetas T C (1996) Three-dimensional simulations of ferromagnetic implant hyperthermia. Med phys, 19(4): 989-997.
[6] Sanda MG, Dunn RL, Michalski J, Sandler HM, Northouse L, Hembroff L. et al (2008) Quality of life and satisfaction with outcome among prostate-cancer survivors. N. Engl. J. Med, 358(12):1250-61.
[7] Sundi D, Jeong BC, Lee SB, Han M (2012) Optimizing the management of high-risk, localized prostate cancer. Korean J. Urol, 53(12): 815-20.
[8] Khor R, Williams S (2013) Contemporary issues in radiotherapy for clinically localized prostate cancer. Hematol. Oncol. Clin. N. Am, 27(6): 1137-62.
[9] Citrin D and Camphausen K A (2013) Biomarkers for prostate: Who will benefit from local treatment, who harbors occult systemic disease and who needs treatment at all? Biomark. Med, 7(6):823-5
[10] Attaluri A, Kandala SK, Wabler M, Zhou H, Cornejo C,Armour M.et al (2015) Magnetic nanoparticle hyperthermia enhances radiation therapy : A study in mouse models of human prostate cancer. Int. J. Hyperth, 31(4): 359-374.
[11]Hassana IM, Attalla EM, El-Gohary M (2022) Assessment of the second cancer risk after Prostate cancer treatment comparison of 3D conformal radiotherapy and intensity modulated radiotherapy. Iran J Med Phys, 19(4): 222-233
[12] HorsmanMR, Overgaard J (2007) Hyperthermia: A potentenhancer of radiotherapy. Clin. Oncol, 19:418-26.
[13] Krawczyk PM, Eppink B, Essers J, Stap J, Rodermond H, Odijk H.et al (2011) Mild hyperthermia inhibits homologous recombination, induces BRCA2 degradation, and sensitizes cancer cells to poly (ADP-ribose) polymerase-1 inhibition. Proc Nati. Acad. Sci. USA, 108(24): 9851-6.
[14] Triantopoulou S, Efstathopoulos E, Platoni K, Uzunoglou N, Kelekis N, Kouloulias V (2013) Radiotherapy in conjunction with superficial and intracavitary hyperthermia for the treatment of solid tumors: Survival and thermal parameters. Clin. Tranl. Oncol, 15: 95-105.
[15] Bergs JW, Krawczyk PM, Borovski T, ten Cate R, Rodermond HM, Stap J. et al (2013) Inhibition of homologous recombination by hyperthermia shunts early double strand break repair to non- homologous end-joining. DNA Repair, 12: 38-45.
[16] Tuul M, Kitao H, Limori M, Matsuoka K, Kiyonari S, Saeki H.et al (2013) Rad9, Rad17, TopBP1 and claspin play essential roles in heat-induced activation of ATR kinase and heat tolerance. PlOS One, 8(2) :e55361.
[17] Roti J L R (2008) Cellular responses to hyperthermia (40-46℃) cell killing and molecular events. Int. J. Hyperth, 24(1): 3-15.
[18] Johannsen M, Thiesen B, Wust P, Jordan A (2010) Magnetic nanoparticle hyperthermia for prostate cancer. Int. J. Hyperth, 26(8): 790-795.
[19] Jordan A, Maier-Hauff K, Wust P, Johannsen M (2006). Nanoparticles for thermotherapy. In : Nanomaterials for cancer therapy, (Kumar CSSR, editor), Wiley-VCH, Weinheim, Germany.
[20] Rand R W, Snow H D, Elliott D G, Snyder M (1981) Thermomagnetic surgery for cancer. Appl Biochem. Biotechnol, 6(4): 265-272.
[21] Dennis CL, Ivkov R (2013) Physics of heat generation using magnetic nanoparticles for hyperthermia. Int. J. Hyperth, 29(8):715-29.
[22] Gu Q, Dockery L. Daniel M C, Bieberich C J, Ma R, Zhu L (2021) Nanoparticle delivery in prostate tumors implanted in mice facilitated by either local or Whole-Body heating. Fluids, 6(8):272
[23] Mahdavi S, Khalafi L, Nikoofar A, Fadavi P, Arbabi Kalateh F, Aryafar T, et al.(2020) Thermal enhancement effect on chemo-radiation of glioblastoma multiform. Int J Radiat Res, 18(2): 255-262.
[24] Mahmoudi K, Bouras A, Bozec D, Ivkov R, Hadjipanayis C (2018) Magnetic hyperthermia therapy for the treatment of Glioblastoma: a review of the therapy's history, efficacy and application in Humans. Int. J. Hyperth, 34(8):1316–1328.
[25] Zhao X, Dong G, Wang C (2021) The non-thermal biological effects and mechanisms of microwave exposure. Int J Radiat Res, 19 (3) : 483-494.
[26] Dewhirst M, Das S, Stauffer P, Craciunescu O, Vujaskovic Z, Thrall D (2011) Hyperthermia. In: Clin. Radiat. Oncol.3e ed, (Gunderson LL, Tepper JE, eds.), Elsevier, Philadelphia (PA), USA.
[27] Sing M (2024) ModifiedPennes bioheat equation with heterogeneous blood perfusion: A newer perspective. Int. J. Heat Mass Transf, 218: 124698.
[28] Rossmanna C, Haemmerich D (2014) Review of temperature dependence of thermal properties, dielectric properties, and perfusion of biological tissues at hyperthermic and ablation temperatures. Crit. Rev. Biomed. Eng, 42(6): 467-492.
[29] Evans S.S, Repasky E.A, Fisher D.T (2015) Fever and the thermal regulation of immunity: The immune system feels the heat. Nat. Rev. Immunol, 15(6), 335–349.
[30] Doaga A, Constantin CP, Cojocariu A, Astefanoaei I, I.Dumitru I, Caltun O F (2011) Phenomenological study of thermal field generated by arrays in hyperthermia as treatment method. J. Adv.Res.Phys, 2(1): 011110.
[31] Bhandari A, Mukharjee S, Kumar A, Singh A, Zhan W (2023) Highlighting the effect of heterogeneous blood perfusion on radio-frequency ablation of human

brain tumors: an image- based numerical investigation. Int. J. Therm. Sci, 189: 108283.

[32] Alamouti A K, Habibi R M, Sharfabadi M M, Lalimi H A (2021) Numerical Study on the effects of blood perfusion and tumor metabolism on tumor temperature for targeted hyperthermia considering a realistic geometrical model of head layers using the finite element method. SN App. Sci, 3: 462.

[33] Jankun J, Keck R W, Skrzypczak-Jankun E, Lilge L, Selman S H (2005) Diverse optical characteristic of the prostate and light delivry system: implications for computer modeling of prostatic photodynamic therapy. BJU Int, 95: 1237-1244.

[34] Pavel M, Stancu A (2009) Study of the optimum injection sites for a multiple metastases region in cancer therapy by using MFH. IEEE Trans. Magn, 45(10) 4825-4828.

[35]Rylander M N, Feng Y, Zhang Y, Bass J, Stafford R J, Volgin A.et al (2006) Optimizing heat shock protein expression induced by prostate cancer laser therapy through predictive computational models. J biomed Opt, 11(4): 041113.

[36] Xu L X, Zhu L, Holmes K R (1998) Thermoregulation in the canine prostate during transurethral microwave hyperthermia, part II: blood flow response, Int. J. Hyperthermia. 14(1): 65-73.

[37] Giering K, Lamprecht I, Minet O, Handke A (1995) Determination of the specific heat capacity of healthy and tumourous human tissue. ThermochimActa, 251: 199-205.

[38] Mcintosh R L, Anderson V (2010) Comprehensive tissue properties database provided for the thermal assessment of a human at rest. Biophys. Rev. Lett, 5(03): 129-151.

[39] Liu A J, Zhou H, Kang W (2013) A numerical study on microwave coagulation therapy. Appl. Math. Sci, 7(104): 5151-5164.

[40] Pennes H H (1948). Analysis of tissue and arterial blood temperatures in the resting human forearm. J. Appl. Physiol, 1(2): 93-122.

[41] Huang, H.W; Horng, T.L (2015) Bioheat transfer and thermal heating for tumor treatment. In: heat transfer and fluid flow in Biological processes, Elsevier, Boston, FL, USA.

[42] Chang I A, Nguyen U D (2004) Thermal modeling of lesion growth with radiofrequency ablation devices. Biomed Eng Online, 3(1): 27-27.

[43] Arcot R, Potts B A, Polascik T J (2021) Focal Cryoablation of image-localized prostate cancer. J Endourol, 35(S2): S17-S23.

[44] Wang J (2014) simulation of magnetic nanoparticle hyperthermia in prostate tumors. Master's thesis in Mechanical Engineering. Baltimore, Maryland : Johns Hopkins University.